

## Long- and short-range electron–hole exchange interaction in different types of quantum dots

This content has been downloaded from IOPscience. Please scroll down to see the full text.

2009 New J. Phys. 11 123024

(<http://iopscience.iop.org/1367-2630/11/12/123024>)

View [the table of contents for this issue](#), or go to the [journal homepage](#) for more

Download details:

IP Address: 128.138.65.115

This content was downloaded on 14/07/2015 at 17:13

Please note that [terms and conditions apply](#).

## Long- and short-range electron–hole exchange interaction in different types of quantum dots

Jun-Wei Luo<sup>1</sup>, Gabriel Bester<sup>2,3</sup> and Alex Zunger<sup>1</sup>

<sup>1</sup> National Renewable Energy Laboratory, Golden, CO 80401, USA

<sup>2</sup> Max Planck Institute for Solid State Research, D-70569 Stuttgart, Germany

E-mail: [g.bester@fkf.mpg.de](mailto:g.bester@fkf.mpg.de)

*New Journal of Physics* **11** (2009) 123024 (12pp)

Received 2 October 2009

Published 21 December 2009

Online at <http://www.njp.org/>

doi:10.1088/1367-2630/11/12/123024

**Abstract.** The electron–hole (e–h) exchange interaction leads to the splitting of the exciton into a pair of bright and a pair of dark states. This bright–dark—or singlet–triplet—exciton splitting was historically calculated as the sum of a long-range (LR) and a short-range (SR) component. Using a numerical atomistic approach, we are able to calculate the exchange integrals as a function of the e–h range of interaction  $S$ , revealing the ‘internal’ structure of the integrals. We apply this procedure to thickness-fluctuation GaAs/AlGaAs quantum dots (QDs), self-assembled InAs/GaAs QDs and colloidal InAs QDs. We find a heterogeneous situation, where the SR component contributes  $\sim 10$ ,  $\sim 20$ – $30$  and  $\sim 20$ – $50\%$  to the total e–h exchange splitting, which is in the range of 10, 100 and 10 000  $\mu\text{eV}$ , for the three types of QDs, respectively. The balance between SR and LR is found to depend critically on the size, shape and type of structure. For all types of QDs we find, surprisingly, a range of interaction, close to the physical dimension of the structures, contributing to a reduction of the integral’s magnitude. These results highlight the complexity of the exchange interaction, warning against simplified models, and establish the basic features of the nature and origin of dark–bright excitonic splitting in QDs.

<sup>3</sup> Author to whom any correspondence should be addressed.

**Contents**

<b>1. Introduction</b>	<b>2</b>
<b>2. Symmetry analysis of exciton states in three prototypical quantum dots (QDs)</b>	<b>3</b>
<b>3. Method of calculation</b>	<b>5</b>
<b>4. Exchange energies versus electron–hole (e–h) interaction radius</b>	<b>6</b>
4.1. Self-assembled QDs . . . . .	6
4.2. Thickness fluctuation QDs (TFQDs) . . . . .	7
4.3. Colloidal QDs . . . . .	8
<b>5. Conclusions and trends</b>	<b>8</b>
<b>6. Summary</b>	<b>11</b>
<b>Acknowledgment</b>	<b>11</b>
<b>References</b>	<b>11</b>

**1. Introduction**

Electron–hole (e–h) interactions in semiconductor quantum dots (QDs) are manifested by a direct Coulomb part, constituting the ‘excitonic-binding energies’ (typically 0.01–0.5 eV) [1], as well as a Coulomb exchange interaction, constituting the ‘dark–bright splitting’,  $\Delta_X$  (typically 0.000 01–0.005 eV) [2]–[4]. The latter interaction—due to the coupling of electron with hole spins—is important for many applications of QDs utilizing the spin degree of freedom in an optical setting [5]. The calculation of this effect is intrinsically difficult because it requires a microscopic treatment. Indeed, an e–h exchange coupling is a consequence of the non-orthogonality of the electron and hole Bloch functions within the crystal unit cell, and must be calculated using an atomistic description for nanostructures containing thousands to hundreds of thousands of atoms.

In model Hamiltonian approaches based on the effective-mass approximation (EMA), the e–h exchange interaction is calculated by a separation of the integral into a short-range (SR) and a long-range (LR) part [6]. This procedure, with its underlying approximations, can lead to analytic expressions for the LR and SR contributions [7]–[9]. For instance, in a zinc-blende spherical nanocrystal of radius  $R$ , with  $T_d$ -point group symmetry, for an exciton derived from a  $\Gamma_6$  electron state and a  $\Gamma_7$  hole state, under the assumption that  $R$  is significantly smaller than the Bohr radius,  $R \ll a_B$ , the exciton splitting  $\Delta_X^{\text{EMA}}$  can be written as [9]

$$\Delta_X^{\text{EMA}} = \pi C \left( \Delta_X^{(b)} + \frac{1}{3} \hbar \omega_{\text{LT}}^{(b)} \right) \left( \frac{a_B}{R} \right)^3, \quad (1)$$

where  $C = 0.672$ ,  $\Delta_X^{(b)}$  is the bulk exchange splitting and  $\hbar \omega_{\text{LT}}^{(b)}$  is the longitudinal-transverse splitting of the bulk exciton. Variations in shape, crystal structure, material, or in the type of exciton addressed (a  $\Gamma_7$  hole state, as assumed above, may be the ground state hole in CuCl, but not in conventional III–V semiconductors) lead to different expressions for equation (1), or prohibit an analytic treatment altogether. Furthermore, the separation into an LR and SR part is only valid for large crystallites and can be questioned for colloidal structures of typically few nm diameter or epitaxial structures with heights of typically 2–5 nm. The fact that the experimental situation is more complex than is usually assumed in the derivation of analytic solutions

(e.g. equation (1)) becomes obvious from the size dependence of  $\Delta_X$ . For InP [11] and InAs [12], a dependence of  $\Delta_X \propto R^{-2}$  was found experimentally in contrast to the  $\Delta_X \propto R^{-3}$  dependence of equation (1). Furthermore, recent experiments on CdSe nanocrystals [10] highlight the discrepancy between exciton models such as that in equation (1) and experiments that call for a more comprehensive theory.

In this work, we wish to establish a description of the e–h exchange bright–dark splitting in QDs that reveals the relative importance of SR and LR effects and their dependence on size, shape and type of structure. This approach will be applied to the three leading forms of semiconductor QDs, with their attendant shapes, compositions and geometries; namely, (i) self-assembled QDs (e.g. InAs in GaAs), (ii) thickness fluctuation QDs (TFQDs, e.g. GaAs in AlGaAs) and (iii) colloidal QDs (e.g. InAs in chemical colloidal suspensions). To this end, we will use an atomistic approach to directly calculate the value of the e–h exchange energies [3, 13] and analyze the results as a function of the range of interaction included in the calculation of the integrals. We find for all three different types of dots a significant contribution from LR interactions. We also find a surprising non-monotonic behavior of the exchange interaction with increasing e–h interaction radius that we explain by an interface effect. This analysis establishes the basic features of the nature and origin of dark–bright excitonic splitting in QDs.

## 2. Symmetry analysis of exciton states in three prototypical quantum dots (QDs)

1. *Self-assembled (Stranski-Krastanov (SK)) QDs* are grown epitaxially under strain conditions leading to island (dot) formation [14]. The QDs are strained, embedded in a (usually) smaller lattice constant material such as InGaAs in GaAs, and have a shape resembling a lens or truncated cone.
2. TFQDs are created by a monolayer fluctuation in the width of a quantum well. In our case (and most experimental cases), the TFQDs are given by the one monolayer fluctuation of a nominally 10-monolayer thick GaAs/Al<sub>0.3</sub>Ga<sub>0.7</sub>As quantum well. The lateral dimension of the TFQD (region where the well is 11-monolayer thick) spans a rectangle with dimensions  $a \times b$ , where  $a$  and  $b$  will be varied between 200 and 400 Å (for more details on this system, see [15]).
3. *Spherical (colloidal) InAs QDs* are precipitates in chemical solutions. We use a spherical overall shape with radii varying between 10 and 35 Å. The surface passivation is performed using an artificial high band gap material surrounding the structure. This approach has been used previously in [16].

In figure 1, we show the exciton splittings expected from group theoretical arguments for the three different prototypes of QDs introduced previously. The symmetry analysis summarized in figure 1(a) shows the results for TFQDs and SK QDs in black and red lines, respectively. The situation for spherical zinc-blende colloidal QDs is shown in figure 1(b). We show a four-step progression leading to the final excitons in columns (iii) and (iv). (i) *Single particle physics*, neglecting both Coulomb and exchange interactions. We show the highest occupied QD state (hole-state) and the lowest unoccupied QD state (electron state). (ii) *Including direct, but neglecting exchange interactions*. This represents a bound e–h pair with artificially high degeneracy following the lack of e–h exchange interaction. (iii) *Including e–h exchange interaction ( $X(K \neq 0)$ )* and keeping the symmetry of the structure unchanged. The dark states in TFQD and SK QDs can be split, since both belong to different irreducible representations.

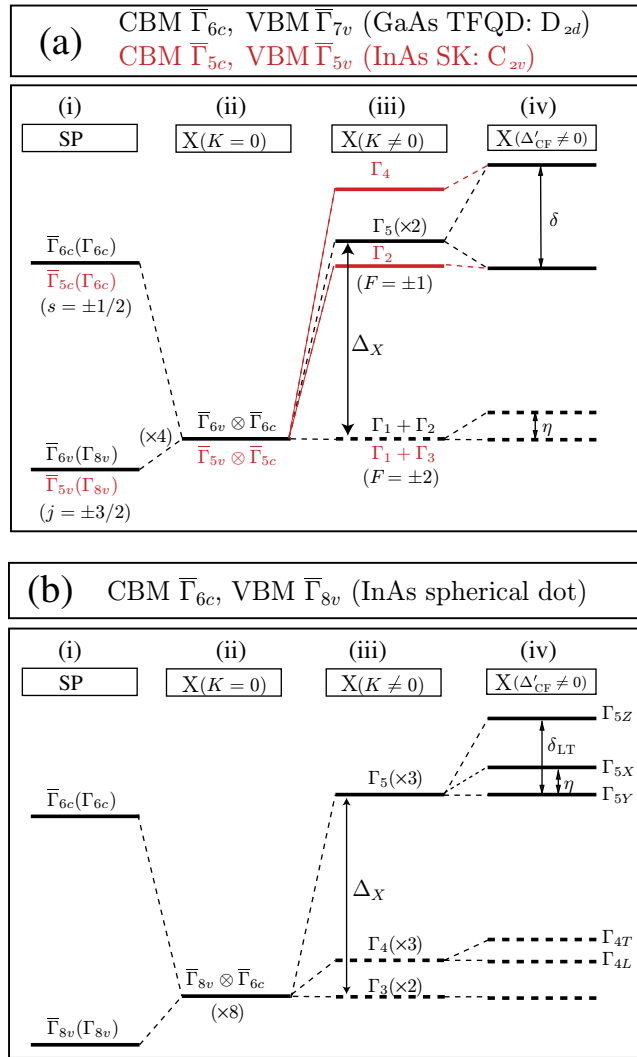


**Figure 1.** Schematic of the evolution of the exciton states for (a) self-embedded InAs/GaAs QDs (text in red) and GaAs TFQD (text in black) and (b) spherical InAs QDs. From the left to the right columns are the single-particle conduction band minimum and valence band maximum states (column (i)), exciton manifold neglecting the exchange interaction (column (ii)), including the exchange interaction (column (iii)), and for reduced symmetry (column (iv)).

In practice, this splitting is very small and not shown graphically. (iv) *Allowing for a lower symmetry*, due to random alloy fluctuations (in the case of QDs made of a semiconductor alloy, such as  $\text{In}_x\text{Ga}_{1-x}\text{As}$ ), an irregular overall shape, or crystal field splittings. The macroscopic shapes of the TFQDs and SK QDs combined with the zinc-blende atomistic symmetry of their crystal lattices lead to the point groups  $C_{2v}$  for SK QDs,  $D_{2d}$  for TFQDs and  $T_d$  for spherical colloidal QDs. The effects mentioned in (iv) can further reduce the symmetry.

Figure 1(a) (gray [red]) shows the evolution of exciton states in SK QDs. The hole states of lens-shaped InAs/GaAs SK QDs are mainly derived from the heavy hole bulk band and have  $\bar{\Gamma}_{5v}$  symmetry. The electron state has  $\bar{\Gamma}_{5c}$  symmetry and the direct product  $\bar{\Gamma}_{5v} \otimes \bar{\Gamma}_{5c}$  leads

to the four irreducible  $C_{2v}$  representations  $\Gamma_1 \oplus \Gamma_2 \oplus \Gamma_3 \oplus \Gamma_4$  [17]. The e–h direct Coulomb interaction lowers all the e–h exciton states by  $\Delta_{\text{coul}}$ , whereas the exchange interactions split  $\Gamma_{2,4}$  from  $\Gamma_{1,3}$  by the exchange energy  $\Delta_X$ . Lowering the symmetry further splits the degenerate exciton states. Note that already at the  $C_{2v}$  level (figure 1(a), column (iii)), all the four states are split, as discussed in [3], the splitting  $\delta$  being referred to as *fine structure*. The focus of this paper is, however, the ‘dark–bright’ splitting  $\Delta_X$ .

Figure 1(a) (black) shows the evolution of *TFQDs with  $D_{2d}$  symmetry*. Both the top hole state (dominant heavy hole,  $J_z = \pm 3/2$  [15]) and the lowest electron state have  $\bar{\Gamma}_6$  symmetry, leading to three irreducible  $D_{2d}$  representations,  $\Gamma_1 \oplus \Gamma_2 \oplus \Gamma_5$ . All the exciton lines are lowered by the direct Coulomb interaction  $\Delta_{\text{coul}}$ . The exchange interactions split the optically active twofold  $\Gamma_5$  states from the optically dark  $\Gamma_{1,2}$ . A further reduction of the symmetry is required for the twofold  $\Gamma_5$  states to split (figure 1(a), column (iv)).

Figure 1(b) shows an equivalent picture for spherical *colloidal InAs QDs*. In the  $T_d$  point group, the e–h exciton consists of the twofold  $\Gamma_{8v}$  hole states and the non-degenerate  $\Gamma_{6c}$  electron state giving rise to the  $\Gamma_3 \oplus \Gamma_4 \oplus \Gamma_5$  exciton states. The exchange interactions split the threefold optically active  $\Gamma_5$  states from the optically dark  $\Gamma_{3,4}$  states. In contrast to  $T_d$  bulk semiconductors [18], where the dark  $\Gamma_4$  states are unsplit from the  $\Gamma_3$  states, our atomistic calculations show a splitting of  $\Gamma_{3,4}$  already for a spherical QD. In lower symmetry (e.g. in an ellipsoidal QD), additional splittings occur (figure 1(b), column (iv)), notably LR exchange splits the longitudinal exciton  $\Gamma_{5L}$  from the transverse excitons  $\Gamma_{5T}$  [18]. Similarly, the  $\Gamma_4$  states are shown to further split into singlet ( $\Gamma_{4L}$ ) and doublet  $\Gamma_{4T}$ .

### 3. Method of calculation

Our approach is to construct an electronic structure theory where the form, range and scaling of the e–h exchange are emerging phenomena rather than a parameterized construction. To this end, the main quantity identifying the QD systems is its single-particle potential  $V_{\text{dot}}(\mathbf{r})$  constructed here from a superposition of overlapping atomic spherical potentials for atom type  $\alpha$ ,  $v_\alpha(\mathbf{r})$ ,

$$V_{\text{dot}}(\mathbf{r}) = \sum_{\alpha} \sum_{\mathbf{r}} v_{\alpha}(\mathbf{r} - \mathbf{R}_{n,\alpha}) + V_{\text{NL}}. \quad (2)$$

The atomic positions  $\{\mathbf{R}_{n,\alpha}\}$  define the shape, size and composition profile, and are relaxed to minimize the strain. The indices  $(\alpha, n)$  extend over the QD and the barrier materials. Both local  $\{v_\alpha\}$  and non-local (spin–orbit)  $V_{\text{NL}}$  potentials are adjusted [19, 20] to correctly reproduce the overall *bulk* properties such as effective masses, critical transition energies, deformation potentials and spin–orbit splittings. Once  $V_{\text{dot}}(\mathbf{r})$  is constructed for a given structure,  $(-\frac{1}{2}\nabla^2 + V_{\text{dot}}(\mathbf{r}))\psi_i = \varepsilon_i\psi_i$  is solved by iterative diagonalization, producing single-particle energies  $\varepsilon_i$  and wavefunctions  $\{\psi_i\}$ . This approach naturally captures the multiband, intervalley and spin–orbit interactions. Once the single-particle states are solved, the many-body problem is set up as a configuration–interaction expansion [21],

$$\langle \Phi_{vc} | H | \Phi_{v'c'} \rangle = (\varepsilon_c - \varepsilon_v)\delta_{v,v'}\delta_{c,c'} - J_{vc,v'c'} + K_{vc,v'c'}, \quad (3)$$

where  $\{\Phi_{vc}\}$  are Slater determinants,  $J$  and  $K$  are the Coulomb and exchange integrals. The latter are given by

$$K_{vc,v'c'}(S) = \sum_{\sigma_1, \sigma_2} \iint \frac{\psi_{v'}^*(\mathbf{r}_1, \sigma_1)\psi_c^*(\mathbf{r}_2, \sigma_2)\psi_{c'}(\mathbf{r}_1, \sigma_1)\psi_v(\mathbf{r}_2, \sigma_2)}{\bar{\epsilon}(\mathbf{r}_1, \mathbf{r}_2)|\mathbf{r}_1 - \mathbf{r}_2|^\theta(S - |\mathbf{r}_1 - \mathbf{r}_2|)} d\mathbf{r}_1 d\mathbf{r}_2. \quad (4)$$

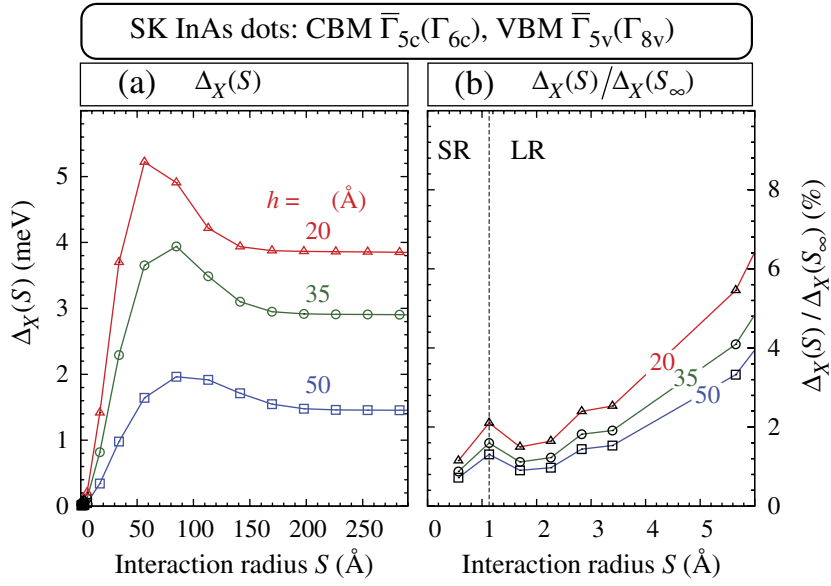


**Figure 2.** (a) Unscreened ( $\bar{\epsilon} = 1$ ) exchange energy  $\Delta_X(S)$  for lens-shaped InAs self-assembled QDs with 250 Å diameter and three different heights,  $h$ , as a function of interaction radius  $S$ . (b) Percentage  $\Delta_X(S)/\Delta_X(S = \infty)$  of the total exchange interaction. The vertical dashed line shows the Wigner–Seitz radius  $R_{WS}$ , which qualitatively separates the SR from the LR contributions of the exchange integrals.

The screening of the e–h interaction is described phenomenologically by the *microscopic*, position-dependent dielectric constant  $\bar{\epsilon}(\mathbf{r})$  [21, 22]. We will also report unscreened results, setting  $\bar{\epsilon}(\mathbf{r}_1, \mathbf{r}_2) = 1$ , to highlight the effect of screening on the e–h exchange interaction. We write  $K$  as a function of the e–h interaction radius  $S$  [13] via a step function  $\theta(S - |\mathbf{r}_1 - \mathbf{r}_2|)$  ( $\theta(x) = 1$  for  $x \geq 0$ , otherwise = 0).

## 4. Exchange energies versus electron–hole (e–h) interaction radius

### 4.1. Self-assembled QDs

Figure 2 shows the results for  $\Delta_X$  (as defined in the third column of figure 1(a)) of three lens-shaped self-assembled InAs/GaAs QDs with 250 Å base diameter and heights of 20, 35 and 50 Å. Figure 2(a) shows  $\Delta_X(S)$  versus the e–h interaction radius  $S$ , whereas figure 2(b) shows the percentage  $\Delta_X(S)/\Delta_X(\infty)$  of the exchange interaction enclosed within the e–h interaction radius  $S$ . We use the electronic Wigner–Seitz radius  $R_{WS} = \frac{a_0}{4} \sqrt[3]{3/2\pi}$  as an attempt to separate the SR from the LR interactions.

We see that with decreasing QD height  $h$ , both the total exchange energy  $\Delta_X(\infty)$  and its SR contribution ( $\Delta_X$  for  $S \leq R_{WS}$ ) increase. The SR contribution to the unscreened exchange energy  $\Delta_X$  does not exceed 2%. However, if screening effects are included, as in equation (4), this value increases to 13%, as a consequence of the microscopic screening function acting mainly on the LR part and leaving the SR part mostly unscreened. Figure 2(a) shows a rapid increase of  $\Delta_X(S)$  versus  $S$  until it reaches a maximum of  $\Delta_X^{\max}(S_0) = 5.2, 3.9$  and 2.0 meV at

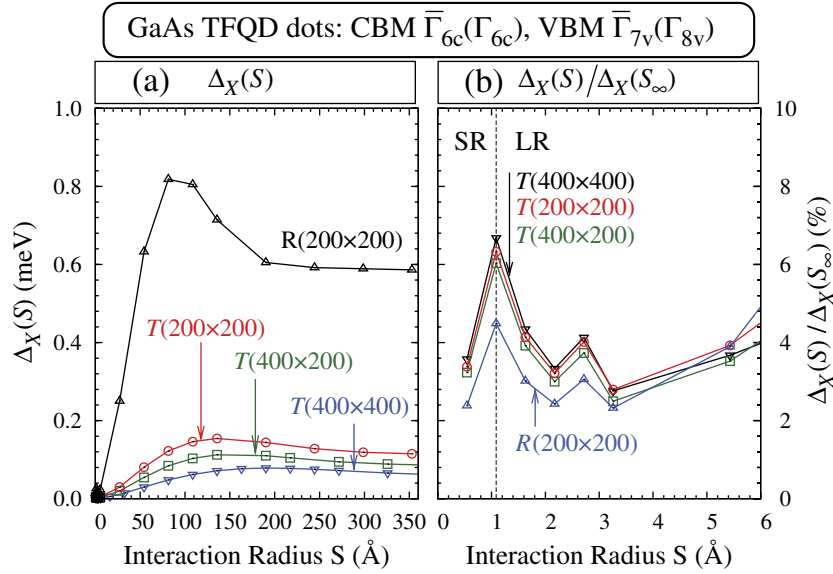


**Figure 3.** (a) Unscrened ( $\bar{\epsilon} = 1$ ) exchange energy  $\Delta_X(S)$  for TFQDs, with height of 31 Å and lateral rectangular sizes of (400 × 400), (400 × 200) and (200 × 200) Å<sup>2</sup> as a function of interaction radius  $S$ . (b) Percentage  $\Delta_X(S)/\Delta_X(S = \infty)$  of the total exchange interaction. The QD labeled (R(200 × 200)) has the same size as the (200 × 200) Å TFQD but is fully embedded in Al<sub>0.3</sub>Ga<sub>0.7</sub>As. The vertical dashed line shows the Wigner–Seitz radius  $R_{WS}$ .

$S_0 \sim 55, 70$  and  $85$  Å for QD heights of 20, 35 and 50 Å, respectively. By further increasing  $S$ , the exchange energy  $\Delta_X(S)$  decreases and finally gradually tends to the asymptotic value  $\Delta_X(S = \infty) = 3.8, 2.9$  and  $1.5$  meV for QD height of 20, 35 and 50 Å, respectively. The overshoot of the integral ( $\Delta_X^{\max}(S_0) - \Delta_X(S = \infty)$ ) decreases with increasing QD height (1.4, 1.0 and 0.5 meV for QD height 20, 35 and 50 Å) and is accompanied by a broadening of the peaks.

#### 4.2. Thickness fluctuation QDs (TFQDs)

Figure 3 shows the exchange energy  $\Delta_X$  versus  $S$  of three GaAs/Al<sub>0.3</sub>Ga<sub>0.7</sub>As TFQDs [15] with lateral rectangular sizes of (200 × 200), (400 × 200) and (400 × 400) Å, respectively. The e–h exchange splitting for the TFQDs (lower part of figure 3(a)) shows an overall behavior similar to the self-assembled QDs (figure 2(a)) but with a magnitude around 30 times smaller. The smaller magnitude is partly due to the low in-plane confinement potential and the leakage of the wavefunctions into the barrier [15]. To illustrate this effect, we have calculated the exchange energy for a GaAs parallelepiped with dimensions 200 × 200 × 31 Å<sup>3</sup> fully embedded in Al<sub>0.3</sub>Ga<sub>0.7</sub>As, i.e. confined to all directions by a conduction (valence) band offset of 264 (151) meV. Figure 3(a) shows a large increase of the exchange energy  $\Delta_X(S = \infty)$  for this QD, labeled R(200 × 200), compared to the TFQD ‘T(200 × 200)’, with the same dimensions. The lower value of the exchange energy in GaAs QDs compared to the InAs QDs is also expected from the EMA (e.g. equation (1)) since the bulk exciton Bohr radius (113 Å in InAs and 368 Å in GaAs) and the longitudinal-transverse splitting is larger in bulk InAs than in bulk GaAs. The SR component of unscrened  $\Delta_X$  (figure 3(a)) is almost 7% (30%, including screening effects)—a

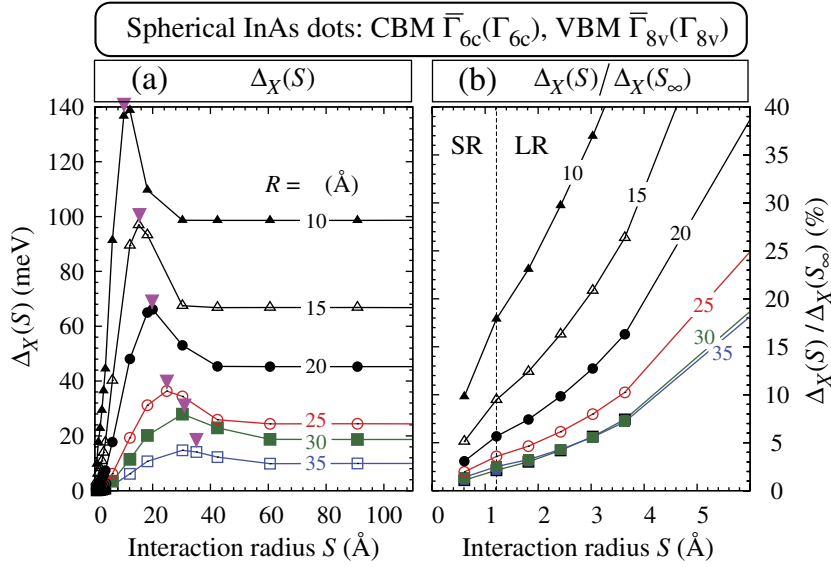


**Figure 4.** (a) Unscrened ( $\bar{\epsilon} = 1$ ) exchange energy  $\Delta_X(S)$  for colloidal spherical InAs QDs with different radii as a function of interaction radius  $S$ . (b) Percentage  $\Delta_X(S)/\Delta_X(S = \infty)$  of the total exchange interaction. The vertical dashed line shows the Wigner–Seitz radius  $R_{WS}$ .

percentage larger than in self-assembled QDs—and shows a pronounced overshoot at the  $R_{WS}$  (dashed line).

### 4.3. Colloidal QDs

We next turn to the spherical InAs *colloidal* QDs (figure 4). Here, we calculated six different spherical InAs QDs with radii varying from 10 to 35 Å in steps of 5 Å. Compared to InAs/GaAs self-assembled QDs and GaAs/AlGaAs TFQDs, these QDs are smaller in size, but have a larger band offset ( $>1$  eV). In figure 4(a), the inverted triangles indicate the respective QDs' radii. The curves show the same qualitative behavior as in figures 2 and 3, but with a larger magnitude. The total exchange energy  $\Delta_X(S = \infty)$  are 98.7, 66.8, 45.2, 24.4, 18.7 and 9.9 meV for  $R = 10, 15, 20, 25, 30$  and 35 Å, respectively, with an overshoot of the exchange energy for an e–h interaction radius  $S$  approximately equal to the QD radius. The overshoot becomes smaller and broader for larger QDs. The fit of the exchange energy  $\Delta_X$  to the expression  $a/R^\lambda$ , leads to the power factors  $\lambda = 2.2$  and  $a = 4948$  meV for  $R$  in Å. This is in good agreement with the experimental value  $\lambda \simeq 2.0$  [12]. The SR contribution to the unscrened exchange energy increases significantly from 2% for the larger QD with  $R = 35$  Å to 18% for the smallest QD ( $R = 10$  Å). This contribution corresponds to 55% for the QD with  $R = 10$  Å, if screening is taken into account (table 1).

## 5. Conclusions and trends

In table 1, we summarize the results given in figures 2–4 and add the screened values of the bright–dark splitting  $\Delta_X$ . The total magnitude of the interaction is given along with its SR contribution (defined by the Wigner–Seitz radius  $R_{WS}$ ). The ratio of the SR component to the

**Table 1.** Screened and unscreened e–h exchange energy splittings ( $\Delta_X$ , see figure 1) in  $\mu\text{eV}$  and Coulomb energy  $\Delta_{\text{coul}}$  in meV for three types of QD. The SR component, the total magnitude and the percentage of the SR part of the bright–dark exchange splittings are tabulated.

Dot type	Dot size	$\Delta_X(S)$ ( $\mu\text{eV}$ )						$\Delta_{\text{coul}}(S)$ (meV)			
		Screened			Unscreened			Screened		Unscreened	
		SR	Total	Ratio (%)	SR	Total	Ratio (%)	SR	Total	SR	Total
SK	h20	35.5	262.4	13.5	80.8	3841.7	2.1	0.169	24.9	0.437	371.8
	h35	20.4	197.0	10.4	46.3	2898.7	1.6	0.100	21.4	0.254	313.9
	h50	8.4	97.8	8.5	19.0	1453.1	1.3	0.039	16.2	0.105	239.9
TFQDs	(200 $\times$ 200)	2.8	8.8	31.8	7.3	115.1	6.3	0.012	11.1	0.034	136.6
	(400 $\times$ 200)	2.0	7.2	27.8	5.2	85.7	6.1	0.008	9.6	0.025	118.3
	(400 $\times$ 400)	1.6	5.2	19.2	4.1	61.2	6.7	0.007	9.0	0.022	112.1
Colloidal	R10	16 750	30 581	54.8	17 655	98 654	17.9	25.2	244.6	21.4	1585.0
	R15	5090	13 358	38.1	6327	66 779	9.5	8.1	156.3	8.3	1154.9
	R20	1879	7034	26.7	2559	45 240	5.7	3.2	105.7	3.9	892.3
	R25	589	3095	19.0	870	24 394	3.6	1.4	75.9	2.3	728.0
	R30	307	2093	14.7	470	18 684	2.5	0.8	60.6	1.5	620.0

total interaction is given in per cent. We added the direct Coulomb interactions  $\Delta_{\text{coul}}$  to the table to highlight the differences between direct and exchange integrals. The analysis of table 1 and figures 2–4 leads to five main conclusions.

1. The *total* (i.e. evaluated for  $S = \infty$ ) e–h exchange energy  $\Delta_X$  in colloidal InAs QDs is at least one order of magnitude larger than in self-assembled InAs/GaAs SK QDs, which, in turn, is at least an order of magnitude larger than in TFQDs. This reveals that the degree of state localization enhanced by quantum confinement is a principal factor in increasing the exchange interactions. In colloidal InAs QDs, electrons and holes are strongly localized inside the QD's interior by the large conduction and valence band offsets, whereas TFQDs have small band offsets of  $\sim 10$  meV (along in-plane directions). The combination of small-sized objects and deep confinement potentials in colloidal QDs, versus large-sized objects with small band offsets in TFQDs, lead to the nearly four orders of magnitude difference in  $\Delta_X$ . The ratio between unscreened and screened total exchange energy  $\Delta_X$  is close to their bulk static dielectric constant ( $\epsilon_0^{\text{InAs}} = 15.2$  and  $\epsilon_0^{\text{GaAs}} = 12.4$  [23]) in SK InAs/GaAs QDs and TFQDs; however, in colloidal InAs QDs it decreases fast from 8.9 to 3.2 as QD size decreases from  $R = 30$  Å to  $R = 10$  Å. The latter effect is the consequence of the size-dependent SR contribution in colloidal structures.
2. For all three types of QDs studied here, we find a balanced situation where both the SR and the LR parts contribute to the exchange integral. Moreover, we find that the balance between SR and LR components changes as a function of size and type of QDs. In general, quantum confinement increases not only the total exchange energy,  $\Delta_X$ , but also the SR component in all three systems. However, using the sole argument of the degree

of localization of the wavefunctions to draw conclusions on the SR–LR balance would be erroneous. Indeed, in TFQDs the degree of localization is significantly smaller than in SK QDs, as discussed above, but the SR component is significantly larger. This observation reveals that the shape and material dependences do not only affect the overall magnitude but also the delicate SR–LR balance of the e–h exchange interaction.

3. For SK QDs and TFQDs, we observe an overshoot of  $\Delta_X(S)$  for an interaction radius close to the Wigner–Seitz radius  $R_{WS}$  in figures 2(b) and 3(b). The reason for this peak might be found in the reciprocal space description [6, 9] of the e–h exchange interaction. The reason is a partial cancellation of the contact part of the analytic (equivalent to SR in real space [7]) and the contact part of the non-analytic ( $\simeq$ LR in real space) exchange splittings. However, while this separation into analytic and non-analytic parts is required for an analytic treatment, the physical insight gained is limited. Our results show that the overshoot of the exchange interaction is related to the degree of macroscopic anisotropy in the wavefunctions. Firstly, the overshoot is not observed for isotropic InAs colloidal QDs. Secondly, it is smaller for the GaAs parallelepiped ( $R(200 \times 200)$ , figure 3(b)), which is fully embedded in  $Al_{0.3}Ga_{0.7}As$  and hence more isotropic than the TFQDs. Thirdly, the overshoot is smaller in the case of fully confined SK QD wavefunctions than in the case of TFQDs with large lateral leakage of the wavefunctions. We conclude that even for e–h interaction distance  $S_{e,h}$  within the Wigner–Seitz cell, the macroscopic extent of the wavefunctions is still a relevant quantity. Furthermore, for wavefunctions with very large in-plane and small out-of-plane dimensions (as in large TFQDs) we expect a large SR contribution that tends to be canceled out by an LR component that slowly develops with the e–h interaction distance.
4. For the three types of QDs, we observe a maximum in  $\Delta_X(S)$  at an interaction radius  $S$  related to the physical dimension of the QDs (figures 2(a), 3(a) and 4(a)). For the spherical colloidal QDs, the QDs’ radii are indicated by invert triangles in figure 4(a) and shown to correspond very well with the positions of the peaks. The overshoot is therefore associated with the distribution of electronic wavefunctions on the QD/barrier interface. Following effective mass theory, the wavefunctions have to satisfy the BenDaniel–Duke [24] boundary condition (i.e.  $m_I^{-1}\nabla\psi_I(\mathbf{r}) = m_O^{-1}\nabla\psi_O(\mathbf{r})$  in which the subscript ‘I’ stands for inside and ‘O’ for outside the QD) across the interface, leading to a significant wavefunction distortion [25]. Additional supporting evidence is that the overshoot shown in figure 4(a) increases with decreasing  $R$ , i.e. when the volume fraction of the interface region increases. The position of the peak represents an effective radius for non-spherical QDs such as lens-shaped InAs/GaAs self-assembled QDs and GaAs TFQDs. We obtain effective radii of 135, 135 and 190 Å for GaAs TFQDs with base sizes of  $(200 \times 200)$ ,  $(400 \times 200)$  and  $(400 \times 400)$  Å, respectively. The effective radii for lens-shaped InAs/GaAs self-assembled QDs are 55, 70 and 75 Å for QD heights of 20, 35 and 50 Å, respectively. The overshoot of the LR exchange term had not been foreseen, but is not in disagreement with previous work [13]. Franceschetti *et al* [13] showed that for spherical InP, CdSe and GaAs QDs of approximately 20 Å radius the multipole expansion of the LR term has not only dipole–dipole contributions, but also monopole–monopole and monopole–dipole components. These components can contribute positively and negatively to the magnitude of the integral, leading to the observed behavior as a function of interaction radius.

5. The e–h exciton binding energy  $\Delta_{\text{coul}}$  is naturally dominated by the LR direct Coulomb interaction. Table 1 shows that in both SK QDs and TFQDs, the SR contribution to total  $\Delta_{\text{coul}}$  is less than 1%. The SR direct Coulomb component increases as QD size decreases. In colloidal InAs QDs, the SR contribution increases from 1 to 10% as QD size decreases from  $R = 30 \text{ \AA}$  to  $R = 10 \text{ \AA}$ . In the envelope-function approximation, assuming an infinite potential barrier at the surface of the QD and a size-independent dielectric constant, one would expect the size-scaling exponent  $\lambda_{\text{coul}} \sim 1$  ( $\Delta_{\text{coul}} \propto R^{-\lambda_{\text{coul}}}$ ). We find  $\lambda_{\text{coul}} = 1.4$  for InAs QDs (see table 1). The deviations from the  $1/R$  scaling are primarily due to the electron and hole wavefunctions ‘spilling out’ of the QD as the size becomes smaller [26].

## 6. Summary

We have calculated the e–h exchange bright–dark splitting for three different common types of QD using an atomistic methodology. The numerical method employed enables us to truncate the interaction after a certain cut-off radius and study the SR and LR nature of the interaction. We first show that from group theory arguments the expected splittings are qualitatively different for all three types of QD. We then analyze the numerical results to draw several conclusions. (i) The e–h integrals vary by more than three orders of magnitude for the three different types of QD as a consequence of the differences in sizes and confinement potentials. (ii) Quantum confinement increases the SR contribution to the integral within one QD type. Across QD types, no such simplification can be made and factors such as shape and the underlying band structure become relevant. For instance, TFQDs have a larger SR component than SK QDs. (iii) For SK QDs and TFQDs, we observe an overshoot of  $\Delta_X(S)$  for an interaction radius close to the Wigner–Seitz radius. We related this effect to the degree of macroscopic anisotropy in the structure. No overshoot is observed in spherical structures. (iv) For the three types of QD, we observe a pronounced maximum in  $\Delta_X(S)$  at an interaction radius  $S$  representing the physical dimension of the QDs. This result shows that the exchange integral is not a purely cumulative quantity (when the interaction radius is increased the magnitude of the integral increases), but has positive as well as negative contributions. We attribute the pronounced maximum to the effect of wavefunction distortions at the interface of the QDs. (v) We find for colloidal InAs QDs a scaling of the exchange integrals  $\propto R^{-2.2}$  and of the direct Coulomb integrals  $\propto R^{-1.4}$ .

## Acknowledgment

Work at NREL was funded by the US Department of Energy, Office of Science, Basic Energy Science, Materials Sciences and Engineering Division, under Contract No. DE-AC36-08GO28308 to NREL.

## References

- [1] Brus L E 1984 *J. Chem. Phys.* **80** 4403
- [2] Bayer M, Ortner G, Forchel A, Hawrylak P and Fafard S 2002 *Physica E* **13** 123
- [3] Bester G, Nair S and Zunger A 2003 *Phys. Rev. B* **67** 161306
- [4] Furis M, Htoon H, Petruska M A, Klimov V I, Barrick T S and Crooker A 2006 *Phys. Rev. B* **73** 241313
- [5] Li X, Wu Y, Steel D, Gammon D, Stievater T H, Katzer D S, Park D, Piermarocchi C and Sham L J 2003 *Science* **301** 809

- [6] Knox R S 1963 *Theory of Excitons in Solid State Physics* ed F Seitz and D Turnbull (New York: Academic)
- [7] Takagahara T 1993 *Phys. Rev. B* **47** 4569
- [8] Efros A L, Rosen M, Kuno M, Nirmal M, Norris D J and Bawendi M 1996 *Phys. Rev. B* **54** 4843
- [9] Gupalov S and Ivchenko E L 2000 *Fiz. Tverd. Tela* **42** 1976  
Gupalov S and Ivchenko E L 2000 *Phys. Solid State* **42** 2030
- [10] Liptay T J, Marshall L F, Rao P S, Ram R J and Bawendi M G 2007 *Phys. Rev. B* **76** 155314
- [11] Micic O I, Cheong H M, Fu H, Zunger A, Sprague J R, Mascarenhas A and Nozik A J 1997 *J. Phys. Chem. B* **101** 4904
- [12] Banin U 1997 *Superlattices Microstruct.* **22** 559
- [13] Franceschetti A, Wang L W, Fu H and Zunger A 1998 *Phys. Rev. B* **58** R13367
- [14] Bimberg D, Grundmann M and Ledentsov N N 1999 *Quantum Dot Heterostructures* (New York: Wiley)
- [15] Luo J W, Bester G and Zunger A 2009 *Phys. Rev. B* **79** 125329
- [16] Califano M, Bester G and Zunger A 2003 *Nano Lett.* **3** 1197
- [17] Koster G F, Dimmock J O, Wheeler R G and Satz H 1963 *Properties of the Thirty-Two Point Groups* (Cambridge, MA: MIT Press)
- [18] Rossler U and Trebin H-R 1981 *Phys. Rev. B* **23** 1961
- [19] Wang L W and Zunger A 1995 *Phys. Rev. B* **51** 17398
- [20] Wang L W, Kim J and Zunger A 1999 *Phys. Rev. B* **59** 5678
- [21] Franceschetti A, Fu H, Wang L-W and Zunger A 1999 *Phys. Rev. B* **60** 1819
- [22] Resta R 1977 *Phys. Rev. B* **16** 2717
- [23] Madelung O 1996 *Semiconductors—Basic Data* 2nd revised edn (Berlin: Springer)
- [24] BenDaniel D J and Duke C B 1966 *Phys. Rev.* **152** 683
- [25] Luo J W, Li S S, Xia J B and Wang L W 2006 *Appl. Phys. Lett.* **88** 143108
- [26] Franceschetti A and Zunger A 1997 *Phys. Rev. Lett.* **78** 915